Research Article

Magnetic Resonance in Chemistry

Received: 25 March 2012 Revised: 22 May 2012 Accepted: 24 May 2012 Published online in Wiley Online Library: 8 July 2012

(wileyonlinelibrary.com) DOI 10.1002/mrc.3836

# Multidimensional solid-state NMR studies of the structure and dynamics of pectic polysaccharides in uniformly $^{13}$C-labeled *Arabidopsis* primary cell walls

**Marilu Dick-Perez,[a] Tuo Wang,[a] Andre Salazar,[b] Olga A. Zabotina[b] and Mei Hong[a]***

**Plant cell wall (CW) polysaccharides are responsible for the mechanical strength and growth of plant cells; however, the high-resolution structure and dynamics of the CW polysaccharides are still poorly understood because of the insoluble nature of these molecules. Here, we use 2D and 3D magic-angle-spinning (MAS) solid-state NMR (SSNMR) to investigate the structural role of pectins in the plant CW. Intact and partially depectinated primary CWs of *Arabidopsis thaliana* were uniformly labeled with $^{13}$C and their NMR spectra were compared. Recent $^{13}$C resonance assignment of the major polysaccharides in *Arabidopsis thaliana* CWs allowed us to determine the effects of depectination on the intermolecular packing and dynamics of the remaining wall polysaccharides. 2D and 3D correlation spectra show the suppression of pectin signals, confirming partial pectin removal by chelating agents and sodium carbonate. Importantly, higher cross peaks are observed in 2D and 3D $^{13}$C spectra of the depectinated CW, suggesting higher rigidity and denser packing of the remaining wall polysaccharides compared with the intact CW. $^{13}$C spin–lattice relaxation times and $^{1}$H rotating-frame spin–lattice relaxation times indicate that the polysaccharides are more rigid on both the nanosecond and microsecond timescales in the depectinated CW. Taken together, these results indicate that pectic polysaccharides are highly dynamic and endow the polysaccharide network of the primary CW with mobility and flexibility, which may be important for pectin functions. This study demonstrates the capability of multidimensional SSNMR to determine the intermolecular interactions and dynamic structures of complex plant materials under near-native conditions. Copyright © 2012 John Wiley & Sons, Ltd.**

*Supporting information may be found in the online version of this article.*

**Keywords:** pectic polysaccharides; solid-state NMR

## Introduction

The cell walls of higher plants are important for the morphology, ionic balance, growth and development of plant cells. Their energy-rich polysaccharides make them potentially alternative energy sources to petroleum and coal. Elucidating the molecular structure and dynamics of plant CW polysaccharides is thus important both for fundamental advances in plant biochemistry and for economic reasons.[1] Plants have a thin primary cell wall laid down by growing cells and a thick secondary wall laid down after termination of cell growth during cell differentiation.[2] The common major biopolymers in primary cell walls are cellulose, hemicelluloses, pectic polysaccharides, and structural glycoproteins. The secondary CWs often show more specialized compositions but generally contain higher levels of cellulose, much less or no pectins, and significant amounts of lignin and hydroxycinnamic acids.

Decades of extraction-based chemical analysis, enzymatic hydrolysis, and microscopic imaging and X-ray diffraction have revealed the chemical composition and ultrastructural details of the insoluble plant CW.[3–5] Pectic polysaccharides are solubilized by chelating agents and contain a mixture of acidic polysaccharides rich in galacturonosyl residues and neutral polysaccharides such as arabinan and galactan. In dicotyledonous flowering plants, the main pectic polysaccharides include homogalacturonan (HGA) and rhamnogalacturonan (RG) I and II.[6] Alkali extraction results in a hemicellulose fraction, which, in dicots, mainly consists of xyloglucan (XG) and small amounts of glucoronoarabinoxylan and galactomannan. Xyloglucans are glucan chains decorated with xylose (Xyl), galactose (Gal), and fucose (Fuc) side chains. Pectins and hemicelluloses constitute the amorphous matrix of the CW, whereas cellulose microfibrils provide the crystalline core. The cellulose microfibrils have diameters of 3–5 nm in primary CWs[7] and can only be hydrolyzed either enzymatically or by heating in strong acid solution.

Although chemical extraction allows quantification of CW components, it is complicated by the partial and non-specific nature of bond cleavage, and the destruction of the physical interactions

* *Correspondence to: Mei Hong, Department of Chemistry and the Ames Laboratory, Iowa State University, Ames, IA 50011, USA. E-mail: mhong@iastate.edu*

a *Department of Chemistry and the Ames Laboratory, Iowa State University, Ames, IA, USA*

b *Department of Biochemistry, Biophysics and Molecular Biology, Iowa State University, Ames, IA, USA*

among the polysaccharides prohibits the elucidation of the native three-dimensional structure of the plant CWs. The main structural techniques, electron microscopy and X-ray diffraction, preferentially detect crystalline cellulose microfibrils but not the amorphous matrix polysaccharides. Two-dimensional solution NMR methods have been used to study lignin-containing secondary cell walls that were solubilized by ball milling, dissolution in organic solvents, and acetylation.[8,9] Although this approach provides relatively native structural information, the sample preparation procedure still causes partial bond cleavage such as to the glycosidic linkage and $\beta$-aryl ethers in lignins. Because of these limitations, the molecular structures and interactions of the polysaccharides in *intact* plant CWs have remained scarce.[4,10,11]

Recently, we began to investigate the molecular structure and dynamics of polysaccharides in insoluble plant CWs using multidimensional solid-state NMR (SSNMR) spectroscopy.[12] SSNMR detects the atomic-resolution structure and dynamics of disordered solids. High-resolution 2D and 3D MAS correlation NMR has been instrumental in the structure determination of insoluble proteins such as membrane proteins and amyloid fibrils,[13–16] but it had not been applied to plant cell walls because of the low sensitivity of $^{13}$C NMR of natural materials. By $^{13}$C-labeling whole plants during growth, we achieved sufficiently high sensitivity to measure 2D and 3D $^{13}$C correlation spectra, which allowed us to assign the $^{13}$C resonances of most CW polysaccharides. Our study focuses on the primary CW of the model plant *Arabidopsis thaliana*, which is the first sequenced plant genome.[17] A large number of *Arabidopsis* mutants are available, thus permitting the study of the effects of individual polysaccharides on CW structure and function. Primary walls (type I) have similar structures and properties among various dicots and non-graminaceous monocots,[18] thus results obtained from *Arabidopsis* are applicable to other higher plants. Our first multidimensional SSNMR study confirmed and refined many $^{13}$C chemical shifts that had been previously obtained from purified cellulose and hemicelluloses.[19–22] We quantified the mobilities of these polysaccharides by measuring NMR relaxation times and dipolar order parameters.[12] The data showed that pectic polysaccharides are the most dynamic species in the CW, whereas hemicelluloses exhibit mobilities intermediate between cellulose and pectins.[12,23] In addition to wild-type primary CW, we also investigated an XG-deficient mutant CW, which was generated by crossing homozygous *xxt1xxt2*[24] and *xxt2xxt5* double knockout lines. The *xxt1xxt2* double mutant was previously reported to have no detectable XG content,[24] whereas the *xxt5* single mutant had significantly lower amounts of XG.[25] The triple knockout mutant has drastically reduced amounts of glycosyl residues typically assigned to XG, such as 4,6-glucose (Glc), t-Xyl, 2-Gal, and t-Fuc.[12] The XG-deficient mutant CW showed much higher mobility for all polysaccharides, indicating the rigidifying influence of hemicelluloses on the polysaccharide network.

Our previous NMR study reported multiple intermolecular cross peaks between pectins and cellulose microfibrils but found only limited correlations between XG and cellulose, which argue against the prevailing model that XG coats the surface of cellulose microfibrils.[26] However, because of the chemical similarity between the glucan backbone of XG and cellulose, it is possible that cellulose-hemicellulose correlations may be difficult to resolve even in 3D $^{13}$C-$^{13}$C-$^{13}$C correlation spectra. At the same time, we observed many cellulose-pectin correlations, which suggest a more central role for pectins in the CW. Pectins are known to have diverse functions in plants: they regulate cell growth, morphology, defense, cell–cell adhesion, wall porosity, and signaling.[27] Thus, it is important to further elucidate the structure and function of pectins in the primary CW.

In this study, we investigate the structure and dynamics of pectic polysaccharides in the primary CW by comparing the $^{13}$C spectra and relaxation times of a partially depectinated CW sample with those of the intact CW and XG-depleted mutant CW. We show by 2D and 3D correlation spectra that chelating agents and sodium carbonate removed a substantial portion of pectic polysaccharides and resulted in altered intermolecular contacts and mobilities for the remaining polysaccharides. We discuss these results in the context of an integrated structural model of the primary CW.

## Experimental Section

### Plant material

Three CW samples of *Arabidopsis thaliana* were prepared: an intact wild-type CW, a depectinated wild-type CW, and a *xxt1xxt2xxt5* triple knockout mutant CW that lacks xyloglucan. The CW material was prepared as described recently.[12] Briefly, *Arabidopsis* plants were germinated, shaken, and grown at 21 °C in the dark in a liquid culture with uniformly $^{13}$C-labeled glucose as the only carbon source (5 g/l). After 14 days, whole seedlings, including roots and hypocotyls, were harvested and homogenized. Alcohol-insoluble residues were extracted with 80% v/v ethanol, washed with a chloroform: methanol (1 : 1) solution to remove lipids and other non-polar compounds. The alcohol-insoluble residues were suspended in 50 mM sodium acetate buffer (pH 5.2) containing 1.5% of SDS and 5 mM sodium metabisulfate to remove most of the intracellular proteins and low-molecular weight compounds. SDS treatment does not remove some of the structural proteins that are crossed-linked with polysaccharides in CWs. Starch was removed by incubation with $\alpha$-amylase for 48 h in the presence of 0.01% thimerosal. The purified CW material was washed with water to remove the digested starch, then washed with acetone and air-dried.

To extract pectin from the wild-type CW, we suspended the purified CW (10 mg/ml) in 50 mM ammonium oxalate (pH 5.0) and incubated it overnight while shaking at room temperature. Ammonium oxalate chelates calcium ions, thus solubilizing pectic polysaccharides containing stretches of unesterified homogalacturonan (HGA). The solubilized pectins were separated from insoluble residue by centrifugation at 10 000 *g* for 20 min. The pellet was washed with deionized water, centrifuged again, and the supernatant was discarded. The pellet was next suspended in 50 mM sodium carbonate (pH 10) and incubated overnight while shaking at room temperature to remove branched RG I, RG II, and esterified HGA. Solubilized pectins were separated by centrifugation at 10 000 *g* for 30 min. The pellet was washed several times with deionized water, every time pelleting by centrifugation at the same force, until the pH of the supernatant reached 5.5–6.0. After these extractions, the part of pectins that loosely bound within the CW, mainly through ionic interactions with $Ca^{2+}$, is largely removed, whereas pectins tightly bound to cellulose and hemicelluloses should remain.

To determine the amount of pectins remaining after extraction with the chelating agent and sodium carbonate, we measured the monosaccharide compositions of untreated and treated CWs. For this analysis, 1 mg of dry CW material was hydrolyzed

with 2 M trifluoroacetic acid (TFA) for 2 h at 120 °C. TFA was evaporated at 50 °C under a stream of air and the pellet was resuspended in 200 μl of water. The resulting solution of monosaccharides was analyzed using high-performance anion exchange chromatography as described before.[28] Monosaccharide standards were purchased from Sigma-Aldrich and included L-Fuc, L-rhamnose (Rha), L-arabinose (Ara), D-Gal, D- Glc, D-Xyl, D-mannose (Man), D-galacturonic acid (GalA), and D-glucuronic acid (GlcA).

About 30 mg of each dry CW sample was rehydrated to 45% (w/w) in a pH 7.5 phosphate buffer and packed into 4 mm MAS rotors for SSNMR experiments.

### Solid-state NMR experiments

Most $^{13}C$ MAS spectra were measured on a Bruker Avance 600 (14.1 Tesla) spectrometer operating at resonance frequencies of 600.13 MHz for $^{1}H$ and 150.9 MHz for $^{13}C$. A double-resonance 4 mm MAS probe was used. Typical radiofrequency (rf) field strengths were 62–70 kHz for $^{1}H$ decoupling and 50 kHz for $^{13}C$ pulses. MAS frequencies ranged from 7 to 12 kHz. $^{13}C$ chemical shifts were referenced to the $^{13}CO$ signal of α-glycine at 176.49 ppm on the TMS scale.

Initial transverse $^{13}C$ magnetization was created using $^{1}H$-$^{13}C$ cross polarization (CP) for experiments that preferentially detected the signals of rigid polysaccharides and by $^{13}C$ direct polarization (DP) for experiments that enhanced the signals of mobile polysaccharides. Recycle delays ranged from 1.5 to 25 s. The long recycle delays were used in $^{13}C$ DP experiments to obtain quantitative intensities for each type of $^{13}C$ in the mixture.

Several 2D and 3D $^{13}C$ correlation experiments (Table S1) were carried out to assign the polysaccharide resonances. A dipolar double-quantum (DQ)-filtered 2D correlation experiment was used to identify predominantly one-bond $^{13}C$ correlation peaks of relatively rigid species. In this experiment, the SPC5 sequence[29] was used to recouple the $^{13}C$-$^{13}C$ dipolar interaction under MAS to mediate polarization transfer. A 2D $^{13}C$ double-quantum J-INADEQUATE experiment[30] was used to detect the signals of mobile polysaccharides. The pulse sequence involves $^{13}C$ direct excitation, a Hahn-echo period for J-coupling mediated polarization transfer, and a short recycle delay of ~2.0 s.[12] The $\omega_1$ dimension of the INADEQUATE spectrum is the sum chemical shift of the two correlated spins, whereas the $\omega_2$ dimension shows the regular single-quantum (SQ) chemical shifts. A 3D CCC experiment[31] containing two spin-diffusion mixing periods, $t_{m1}$ and $t_{m2}$, was used to further resolve cross peaks. The $t_{m1}$ was short (8 ms) to observe intramolecular cross peaks, whereas $t_{m2}$ was long (300 ms) to observe both intramolecular and intermolecular correlations.

2D $^{13}C$ spin diffusion (DARR or PDSD) correlation experiments[32] were performed to obtain through-space correlation signals. The $^{13}C$ mixing times were 8 ms and 300 ms. To investigate the mobility of the CW polysaccharides, we conducted a $^{1}H$ $T_{1\rho}$-filtered spin diffusion experiment on the intact CW where a $^{1}H$ spin-lock period was added before $^{1}H$-$^{13}C$ CP, and a spin diffusion mixing time of 300 ms was used. The $T_{1\rho}$-filtered 2D spectrum was compared with the unfiltered spectra of both the intact and depectinated CWs. A series of 1D $^{1}H$ $T_{1\rho}$ filtered experiments with varying $^{1}H$ spin-lock times were used to optimize the filter time for the 2D experiment.

$^{13}C$ $T_1$ and $^{1}H$ $T_{1\rho}$ relaxation times were measured to investigate the mobility of the polysaccharides in the depectinated CW.[12] For the $^{13}C$ $T_1$ experiment, a standard inversion recovery sequence with $^{13}C$ DP was used in conjunction with long recycle delays to obtain quantitative intensities. The recycle delay was 25 s for the intact and depectinated CW samples and 10 s for the XG-deficient triple mutant CW. These values were chosen based on the previously measured $^{13}C$ $T_1$ values, which were less than 1 s for the triple mutant CW and less than 4 s for the wild-type CW.[12] The $^{1}H$ $T_{1\rho}$ was measured using a variable Lee-Goldburg spin-lock period before a constant $^{1}H$-$^{13}C$ CP period, which also involved Lee–Goldburg spin lock on the $^{1}H$ channel. As a result, the $^{1}H$ $T_{1\rho}$ is site-specific. Both $^{13}C$ $T_1$ and $^{1}H$ $T_{1\rho}$ relaxation data were fit using the KaleidaGraph software using double-exponential functions.

## Results and Discussion

*Arabidopsis thaliana* seedling grown in liquid medium in the dark for 14 days develops strongly elongated hypocotyl with closed cotyledons and very short root. It was demonstrated[33] that only by the fourth week of growth does the *Arabidopsis* hypocotyl undergo secondary thickening, when cell divisions in the central cylinder give rise to the secondary xylem, the vascular cambium, and the secondary phloem. This differentiation follows the cessation of the elongation phase. Thus, the CW material used in our study contains mostly primary CWs from elongating hypocotyl, which contains epidermal, cortical, and endodermal cells, with very low amount of secondary CW from the hypocotyl's undeveloped vascular tissues and insignificant contribution of root tissues. The use of homogenized etiolated seedlings allows us to obtain information about the average CW structure instead of the CW of a single cell type. Structural differences among specialized CWs can be investigated in a tissue-specific manner in the future.

The depectination procedure[18] was chosen to avoid extraction of hemicellulosic polysaccharides and preserve cellulose-hemicellulose interactions. Indeed, monosaccharide analysis after depectination (Table 1) confirms that Rha and GalA amounts are significantly reduced by the treatment, whereas the percentages of monosaccharides usually found in hemicelluloses, such as Xyl, Fuc, and Gal, are largely unaffected. The second column of Table 1 shows the monosaccharide percentages of the treated CW normalized to a total amount of 100%. Because the loss of some sugars necessarily increases the percentages of the others, we also compared the ratios of various monosaccharides to Glc because most Glc exists in cellulose and hemicellulosic XG, which is minimally affected by the extraction procedure. Table 1 shows that Rha and GalA are reduced to 40–55% of the levels of the untreated CW, whereas the Ara content is reduced to ~79%. In comparison, the amounts of Xyl, Fuc, and Gal are little affected. Thus, the depectination procedure removed significant amounts of RG and HGA while retaining hemicelluloses. The fact that a small amount of RG and HGA still remains may result from their partial association with hemicellulose and cellulose through covalent or hydrogen bonds. Further removal of pectins in the CW, for example, by enzymatic breakdown of HGA, is possible. To simplify the analysis below, we call this partially extracted CW as depectinated CW.

### 2D and 3D $^{13}C$ correlation spectra of depectinated versus intact cell walls

We examined the structural role of pectin in the primary wall by comparing the 1D, 2D, and 3D $^{13}C$ MAS spectra of depectinated and intact CWs. Figure 1 shows quantitative 1D $^{13}C$ DP spectra

**Table 1.** Monosaccharide percentages in intact and depectinated cell walls. Sugar residues whose percentages are significantly reduced by depectination are bolded

| Sugar | Untreated CW | Depectinated CW | Ratio to Glc, untreated | Ratio to Glc, Depectinated |
|---|---|---|---|---|
| Fucose | 4.3 ± 0.2 | 5.4 ± 0.5 | 0.26 | 0.26 |
| Rhamnose | **11.4 ± 0.2** | **6.0 ± 0.5** | **0.69** | **0.29** |
| Arabinose | **12.3 ± 0.3** | **12.1 ± 0.9** | **0.74** | **0.59** |
| Galactose | 18.8 ± 0.3 | 21.0 ± 1.0 | 1.14 | 1.03 |
| Glucose | 16.5 ± 0.3 | 20.4 ± 1.1 | 1.0 | 1.0 |
| Xylose | 18.7 ± 0.2 | 21.0 ± 1.0 | 1.13 | 1.03 |
| Mannose | 3.8 ± 0.1 | 4.3 ± 0.5 | 0.23 | 0.21 |
| Galacturonic acid | **12.5 ± 0.3** | **8.6 ± 0.7** | **0.75** | **0.42** |
| Glucuronic acid | **1.8 ± 0.1** | **1.1 ± 0.2** | **0.11** | **0.05** |

of the two samples, measured with a long recycle delay of 25 s. The spectra are scaled such that no polysaccharide signals in the depectinated sample exceed the corresponding intensities of the intact CW. This condition is satisfied when the intensity of the interior cellulose C4 peak at 89 ppm is matched between the two spectra, whereas all other polysaccharide signals are lower in the treated CW sample. Thus, the interior cellulose C4 peak provides the reference between the two samples, consistent with the fact that pectin extraction should have minimal impact on the cellulose microfibrils. These 1D $^{13}C$ spectra show that peaks with lower intensities in the depectinated CW indeed mainly correspond to pectin signals. For example, the GalA and Rha C1 peaks at 101 ppm, the Rha C2 and GalA C4 peaks at 80 ppm, and GalA C2 and Rha C5 peaks at 69 ppm have much lower intensities in the depectinated CW than in the intact CW.

To better resolve the $^{13}C$ signals and verify the reduction of pectin, we measured several 2D $^{13}C$-$^{13}C$ correlation spectra. Pectic polysaccharides were previously found to be highly mobile in the intact CW based on $^{13}C$ DP experiments and relaxation times.[12] A 2D DP J-INADEQUATE experiment, which correlates the sum chemical shift of two directly bonded $^{13}C$ spins in the $\omega_1$ dimension with the individual chemical shifts in the $\omega_2$ dimension, is especially effective for detecting the signals of mobile molecules.[12] Figure 2a, b compares the J-INADEQUATE spectra of the depectinated and intact CW samples. The INADEQUATE spectrum does not have a diagonal, thus giving excellent resolution for $^{13}C$ signals with similar chemical shifts. A number of pectin peaks are either weakened or absent (red boxes) in the depectinated CW spectrum. For example, the Ara C1-C2 cross peaks at $\omega_2$ chemical shifts of 110 and 82 ppm (with a $\omega_1$ DQ chemical shift of 192 ppm) and the Ara C4-C5 peaks at $\omega_2$ chemical shifts of 83 ppm and 67 (with a $\omega_1$ DQ chemical shift of 151 ppm) are missing in the depectinated CW spectrum, and the GalA C1-C2 cross peaks at $\omega_2$ chemical shifts of 101 and 68 ppm are much lower in the depectinated spectrum than in the intact CW spectrum. Representative 1D cross sections are shown in Figure S1a, b. These pectin sites have weaker or undetectable intensities *despite* the fact that they are highly dynamic in the intact CW,[12] which should make them easy to detect in the INADEQUATE spectrum. Thus, the intensity loss is strong evidence for the significant removal of these pectins from the cell wall.

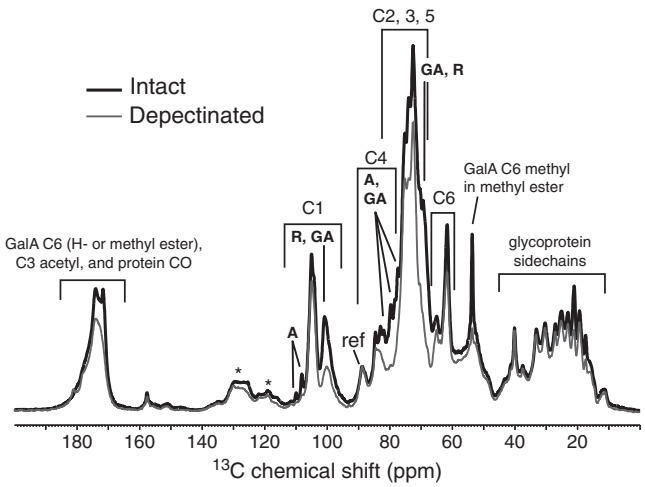


**Figure 1.** Quantitative 1D $^{13}C$ DP-MAS spectra of (a) **intact** and (b) depectinated *Arabidopsis thaliana* cell walls. A long recycle delay of 25 s was used to obtain quantitative intensities. Asterisks denote spinning sidebands. The spectra were measured under 7 kHz MAS at 295 K. Abbreviations of the assignment in this and subsequent figures are defined in Fig. 2a.

Interestingly, we also observed several new cross peaks in the depectinated CW spectrum that were absent in the intact CW spectrum (blue boxes). For example, two cross peaks at $\omega_2$ chemical shifts of 97 and 75 ppm (with a $\omega_1$ DQ chemical shift of 172 ppm) were observed, and another pair at 93 and 72 ppm (with a $\omega_1$ chemical shift of 165 ppm) was also additional to the intact CW spectrum. These resonances have not yet been assigned. They may result from hydrolysis of esters to free carboxylate groups after sodium carbonate treatment at pH 10, or from the higher sensitivity of the remaining polysaccharides in the depectinated wall (see below), which may allow small amounts of polysaccharides to be better detected.

To understand how the partial removal of pectin in the CW affects the remaining polysaccharides, we measured the dipolar DQ-filtered correlation spectra of intact and depectinated CWs (Fig. 2c, d). This experiment uses $^{1}H$-$^{13}C$ CP to establish the initial $^{13}C$ magnetization and $^{13}C$-$^{13}C$ dipolar coupling to mediate polarization transfer; thus, the signals of mobile pectins are weaker than those of cellulose and hemicellulose. Nevertheless, the intact CW spectrum shows a number of well-resolved pectin cross peaks such as Rha C1-C2 (101–80 ppm), C2-C3 (80–71 ppm), and GalA C1-C2 (99–69 ppm), which are clearly suppressed in the depectinated CW spectrum. Figure S1c shows 1D cross sections to further illustrate the fact that these distinct pectin signals are below the detection limit in the treated sample. Similar to the J-INADEQUATE spectra, a few cross peaks such as the interior cellulose C1-C4 cross peak at ($\omega_1$, $\omega_2$) chemical shifts of (105, 89) ppm are higher in the depectinated spectrum than the intact

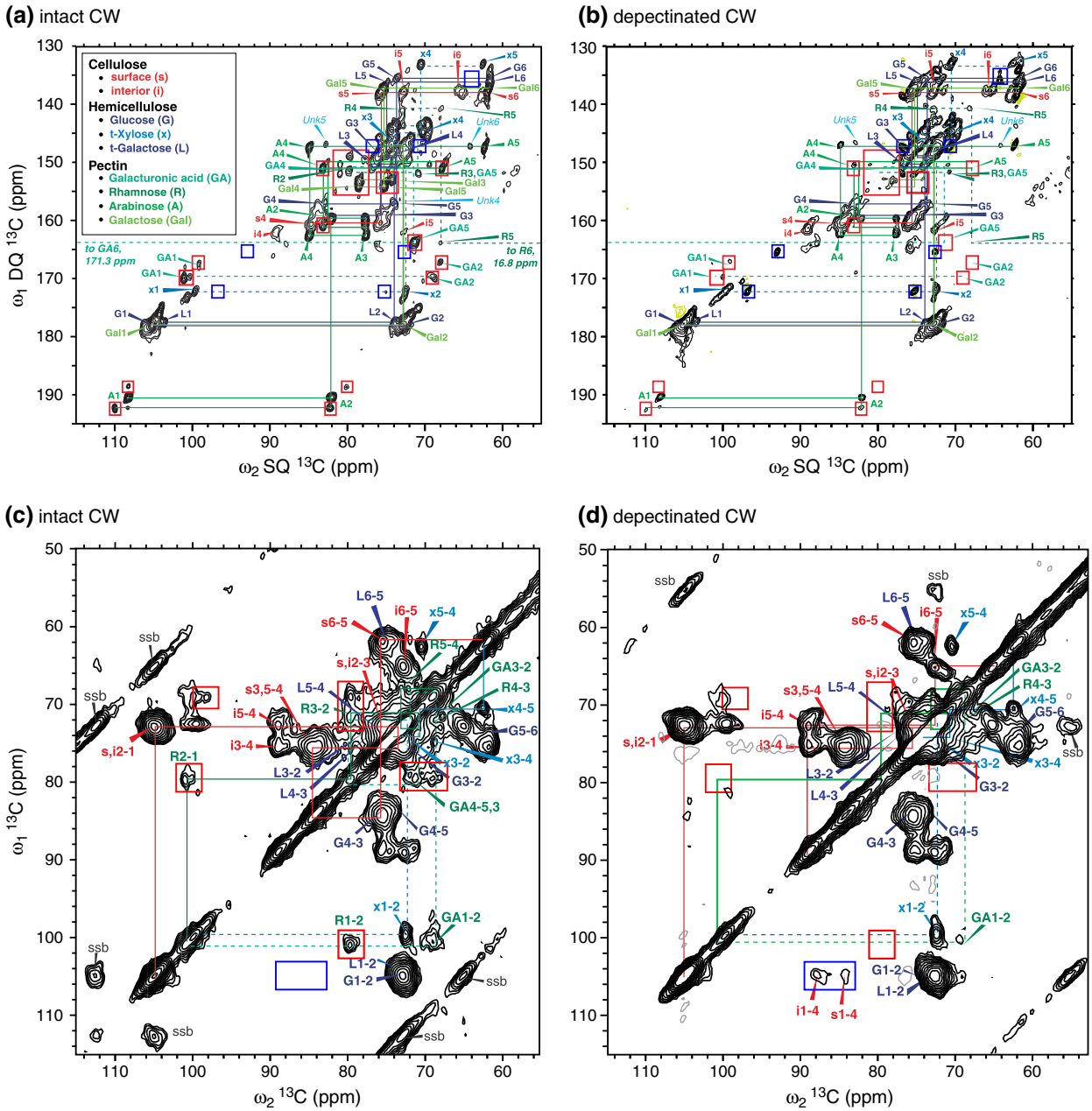


**Figure 2.** 2D $^{13}C$-$^{13}C$ correlation spectra of (a, c) intact and (b, d) depectinated cell walls. (a, b) 2D DP J-INADEQUATE spectra, which preferentially detect the signals of mobile polysaccharides. DQ $^{13}C$ chemical shifts in the $\omega_1$ dimension are correlated with single-quantum $^{13}C$ chemical shifts in the $\omega_2$ dimension. (c, d) 2D CP DQ filtered $^{13}C$ correlation spectra, which preferentially enhance the signals of rigid polysaccharides. Selected signals that are present in the intact CW but absent in the depectinated CW are boxed in red, whereas signals that are weak in the intact CW but strong in the depectinated CW are boxed in blue.

CW spectrum, again suggesting that cellulose microfibrils become more rigid after depectination, thus giving higher polarization transfer efficiencies.

To further verify the partial removal of pectins by ammonium oxalate and sodium carbonate, we measured a 2D $^{13}C$ DARR correlation spectrum, which detects through-space contacts between carbons. With a short mixing time of 8 ms, only intra-residue cross peaks are expected and can result from both relayed transfer through several bonds and direct through-space transfer. Qualitative inspection of the 2D spectra (Fig. 3a, b) suggested no large differences between the intact and depectinated spectra. However, close examination of the 1D cross sections indicate clear changes in the relative intensities of the peaks, with the depectinated CW showing lower intensities at pectin chemical shifts. In comparing the cross sections, we scaled the spectra so that no peak in the treated CW exceeds the intensity of the corresponding peak in the intact CW. For example, in the 80-ppm cross section of Rha C2 and GalA C4 (Fig. 3c), the 105-ppm peak has the highest relative intensity in the depectinated sample and is thus matched to the 105-ppm peak of the intact CW. Normalized in this way, the 80-ppm diagonal peak is much lower in the treated sample, and the 70-ppm peak because of Rha C2-C5 and GalA C4-C2 correlation is also weaker in the depectinated sample. In the 68-ppm cross section of Rha C5

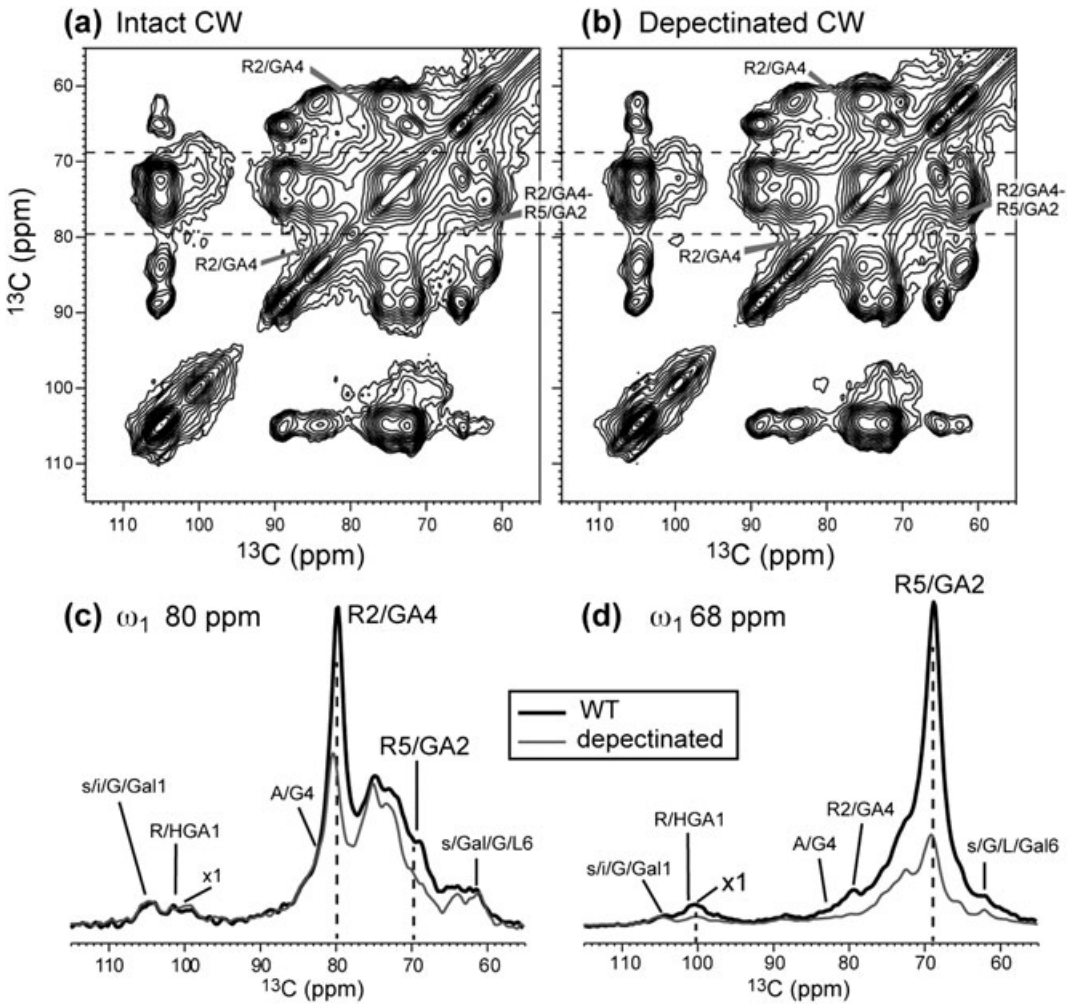


**Figure 3.** 2D $^{13}$C-$^{13}$C DARR spectra of (a) intact and (b) depectinated cell walls with an 8-ms mixing time. (c) 80-ppm $\omega_1$ cross section of Rha C2 and GalA C4. (d) 68-ppm $\omega_1$ cross section of Rha C5 and GalA C2.

and GalA C2 (Fig. 3d), with the cellulose 105-ppm C1 intensity matched between the two spectra, most other intensities are significantly lower in the depectinated CW spectrum. These include cross peaks to Rha or GalA C1 (101 ppm), Xyl C1 (100 ppm), Rha C2 or GalA C4 (80 ppm), and C6 of various polysaccharides (63 ppm). Therefore, all three types of 2D correlation spectra, which enhance the signals of either mobile species or rigid molecules, show lower intensities for the pectin carbons, which indicate that the spectral changes must result from lower amounts of pectins in the CW rather than from mobility changes because the latter should decrease intensities in some spectra while increasing them in others.

For cellulose and hemicellulose, the depectinated CW shows higher intensities than the intact CW in spectra that preferentially enhance the signals of rigid molecules. This change suggests that the partial removal of pectins may increase the rigidity of the remaining polysaccharides, which, in turn, suggests denser packing and stronger intermolecular interactions of the remaining polysaccharides. If this is true, then we should observe stronger intermolecular cross peaks between cellulose and hemicellulose. Intramolecular cross peak intensities should also increase because of enhanced spin diffusion efficiencies. To test these hypotheses, we measured the 3D $^{13}$C-$^{13}$C-$^{13}$C correlation spectrum[31] of the depectinated CW and compared it with that of the intact CW. The two spectra were measured using spin diffusion mixing times of 8 and 300 ms and with CP to generate the initial $^{13}$C polarization. Figure 4 shows that the number and intensities of cellulose and hemicellulose cross peaks in the 3D spectra are indeed higher for the depectinated cell wall (bottom) than the intact cell wall (top). For example, in the 105-ppm $\omega_1$ plane of cellulose and XG Glc C1 (Fig. 4a), a series of strong cross peaks with interior cellulose C4 (89 ppm) and surface cellulose C4 (85 ppm) are observed in the treated sample, whereas the corresponding peaks are weaker in the intact CW sample (Figure S2a). Stronger C1 cross peaks with C6 are also observed. A new cross peak at (105, 72, 100) ppm in the depectinated CW may be assigned to intermolecular correlation among cellulose C1, cellulose C2/3/5, and Xyl C1. In the 89-ppm $\omega_1$ plane of interior cellulose C4 (Fig. 4b), stronger intramolecular cross peaks with 105 ppm (C1), 73 ppm (C3), and 63 ppm (C6) are observed in the depectinated spectrum. In addition, an intermolecular cross peak between interior cellulose C3 and surface cellulose C4 (75 to 85 ppm) is detected, which is absent in the intact CW. In the 84 ppm plane of surface cellulose and XG Glc C4 (Fig. 4c), intermolecular cross peaks between surface and interior cellulose are enhanced in the depectinated CW spectrum. These intensity difference are illustrated in selected 1D slices in Figure S2. In addition, 2D correlation spectra with 300-ms spin diffusion were compared

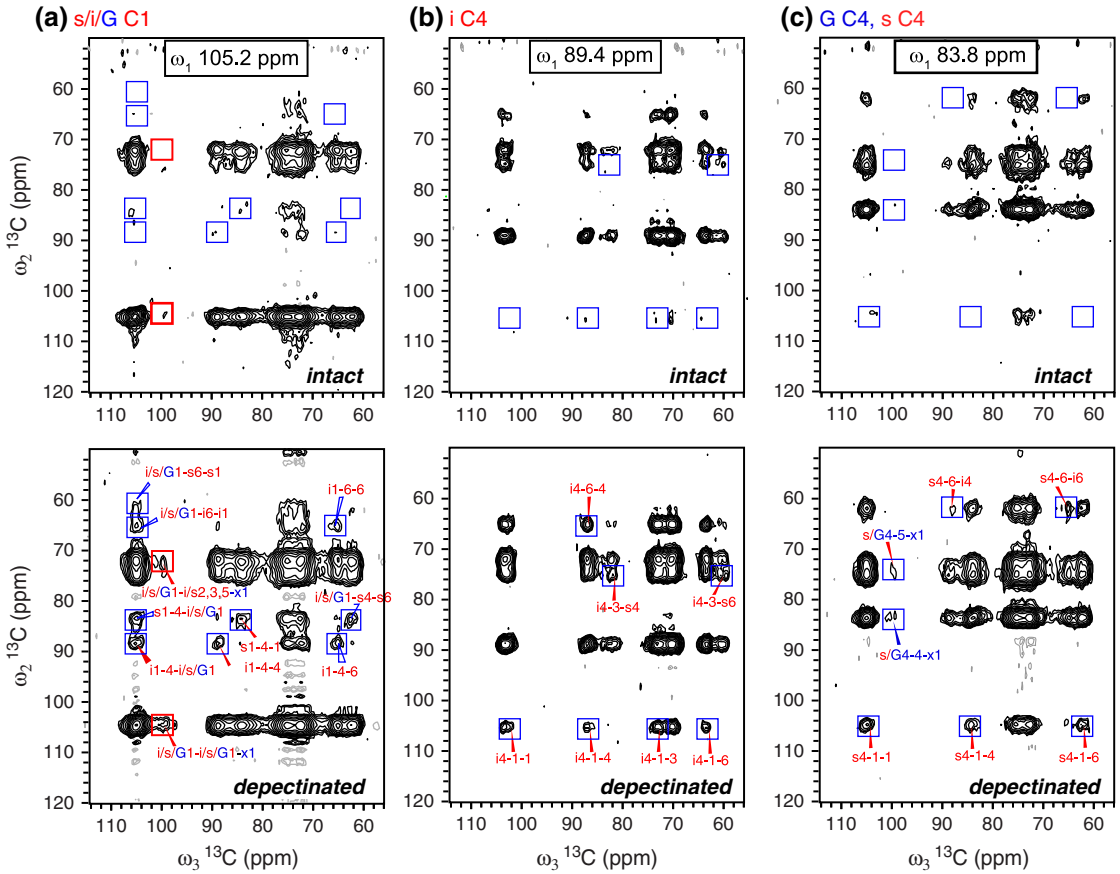


**Figure 4.** Selected 2D cross sections of the 3D CCC spectra of intact (top) and depectinated (bottom) cell walls, measured with spin diffusion mixing times of 8 and 300 ms. (a) 105.2 ppm $\omega_1$ plane of cellulose C1. (b) 89.4 ppm $\omega_1$ plane of interior cellulose C4. (c) 83.8 ppm $\omega_1$ plane of surface cellulose and XG backbone Glc C4. Peaks whose intensities increased in the depectinated sample are boxed in blue.

between the intact and depectinated samples (Figure S3) and confirmed the intensity differences in the 3D spectra.

### Dynamics of the depectinated cell wall from NMR relaxation times

To directly determine if partial depectination increased the rigidity of the wall polysaccharides, we measured the $^{13}C$ $T_1$ and $^{1}H$ $T_{1\rho}$ relaxation times of the depectinated CW and compared them with those of the intact wild-type CW and the XG-depleted triple mutant. To ensure quantitative intensities for all polysaccharides, we measured $^{13}C$ $T_1$ using DP and long recycle delays. Similar to the other two CW samples, $^{13}C$ $T_1$ relaxation of the depectinated CW is double exponential (Figure S4), indicating heterogeneous dynamics for most polysaccharides. Figure 5a plots selected $^{13}C$ $T_1$ relaxation times of the slow-relaxing component of representative peaks of matrix polysaccharides (101, 82, and 69 ppm) and cellulose (88 and 65 ppm). The complete set of $^{13}C$ $T_1$ relaxation times and the relative percentages of the slow- and fast-relaxing components are shown in Fig. 6a-c. The data indicate that the depectinated CW has longer $^{13}C$ $T_1$ relaxation times and higher fractions of the slow-relaxing component than the intact wild-type CW. For example, the $^{13}C$ $T_1$ of the 69-ppm peak of Rha C5 and HGA C2 increased from $0.6 \pm 0.1$ to $2.7 \pm 0.5$ s, whereas the 101-ppm peak of Rha and HGA C1 increased from $1.5 \pm 0.4$ to $2.5 \pm 0.5$ s. The longer relaxation times most likely result from a combination of reduced amplitudes and slower motional rates of the depectinated CW polysaccharides. Our previous measurement of C-H dipolar order parameters of intact CW showed that pectins had the lowest C-H order parameters among all polysaccharides,[12] which were correlated with their fast relaxation rates. Partial removal of the pectins may rigidify the cell wall by decreasing the distances among the remaining polysaccharides. Compared with the matrix polysaccharides, the crystalline core of cellulose, detected through the well-resolved interior cellulose C4 (88 ppm) and C6 (65 ppm) peaks, shows no significant $T_1$ changes between the intact and partially depectinated cell wall, which provides a useful control to the observed dynamic changes of the matrix polysaccharides. In contrast to the effects of pectin removal, the XG-depleted mutant shows drastically and uniformly shortened $^{13}C$ $T_1$'s and much higher fractions of the mobile component for all sites.

The $^{13}C$ $T_1$ relaxation times are influenced by $^{13}C$ spin diffusion, which is efficient for the uniformly $^{13}C$-labeled CW, and are specifically sensitive to nanosecond motion. To determine the dynamics of CW polysaccharides more site-specifically and probe motion on a different timescale, we measured the $^{1}H$ $T_{1\rho}$ relaxation time in a spin-diffusion free fashion using a Lee–Goldburg spin-lock experiment.[12,34] Figures 5b and 6d-f compare the $^{1}H$ $T_{1\rho}$'s of the three CW samples. A similar trend to $^{13}C$ $T_1$ is observed: the depectinated CW exhibits longer $T_{1\rho}$ and higher fractions of the slow-relaxing component, whereas the XG mutant has the shortest $T_{1\rho}$ relaxation times and the highest fractions of the dynamic component. For the matrix polysaccharides,

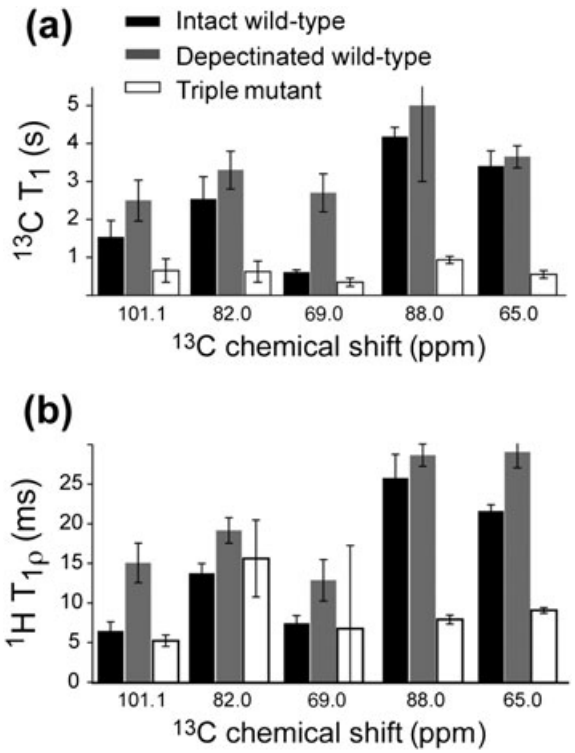


**Figure 5.** Representative $^{13}$C $T_1$ (a) and $^{1}$H $T_{1\rho}$ (b) relaxation times of intact CW (black), depectinated CW (gray), and the XG-deficient triple mutant CW (white). Only the relaxation times of the slow-relaxing components are shown; the full panel of relaxation times is given in Fig. 6. The depectinated CW has significantly longer relaxation times for the matrix polysaccharides (101, 82, and 69 ppm) than the intact CW. The triple mutant CW has the shortest relaxation times along the three samples.

the $T_{1\rho}$ differences between the intact and depectinated CWs are larger than the error bars of the measurement. Therefore, the polysaccharides in the depectinated CW have reduced mobility on both the nanosecond and microsecond timescales compared with the intact CW. Moreover, the common presence of a fast-relaxing component that coexists with a slow-relaxing component cannot be fully attributed to spin diffusion but must partly reflect the intrinsic dynamic heterogeneity of most polysaccharide chains.

Both $^{13}$C $T_1$ and $^{1}$H $T_{1\rho}$ data indicate that cellulose has longer relaxation times than other polysaccharides. The different $^{1}$H $T_{1\rho}$'s can be exploited for spectral editing.[23] Specifically, we can retain the signals of rigid polysaccharides with long $T_{1\rho}$'s while suppressing the signals of mobile polysaccharides by applying a $^{1}$H spin-lock period before $^{1}$H-$^{13}$C cross polarization. Figure 7 shows a series of 1D $^{13}$C CP-MAS spectra measured with $^{1}$H spin lock times from 1 to 7 ms. By 3 ms, the intensities of the mobile polysaccharides are significantly reduced. For example, the 89-ppm C4 peak of the interior cellulose is better retained than the 85-ppm C4 peak of the more mobile surface cellulose. By 7 ms, most glycoprotein sidechain signals between 10 and 40 ppm and the 100-ppm C1 signal of Xyl and GalA are also suppressed.

Based on the 1D $^{1}$H $T_{1\rho}$ spin-lock series, we conducted a $T_{1\rho}$-filtered 2D correlation experiment to selectively detect rigid polysaccharides in the intact CW. We compared this spectrum with the unfiltered spectrum of the depectinated CW to assess if the $^{1}$H $T_{1\rho}$ filter suppresses the same polysaccharide signals as chemical extraction. Figure 8 compares the 2D spectra of the intact CW without the $T_{1\rho}$ filter (black), the intact CW with a 7 ms $T_{1\rho}$ filter (blue), and the depectinated CW without any filter (red). All spectra were measured with the same $^{13}$C spin diffusion time of 300 ms. Representative 1D cross sections are compared in Fig. 8d-f. In general, the depectinated CW spectrum has higher sensitivity than the intact CW spectrum by as much as twofold, whereas the $T_{1\rho}$-filtered spectrum of the intact CW has two to three times lower sensitivity than the unfiltered spectrum of the intact CW. We scaled the unfiltered spectra of the intact and depectinated CW samples such that the intensity of the depectinated sample is not higher than that of the intact CW. In the 105-ppm cross section of cellulose and XG Glc C1 (Fig. 8d), the 89-ppm C4 peak of interior cellulose and the 85-ppm C4 peak, which results from surface cellulose, XG backbone, and Ara, show different relative intensities: the unfiltered spectrum of the intact CW has a higher 89-ppm peak than the 85-ppm peak, whereas the depectinated sample has the opposite situation. Because the 85-ppm peak results from a mixture of polysaccharides, the difference indicates that the depectinated CW has additional intermolecular contacts between cellulose and matrix polysaccharides. The most likely species contributing to the increased 85-ppm peak intensity are XG backbone C4 and the remaining Ara C4. The 65.0-ppm cross section (Fig. 8f) of interior cellulose C6 supports this observation because the depectinated CW shows reduced intensity at 89 ppm compared with the intact CW when the 85-ppm is set to be the same between the two samples.

The $T_{1\rho}$-filtered spectrum of the intact CW has the lowest sensitivity among the three spectra, indicating that not only pectins but also other mobile polysaccharides are suppressed by the spectroscopic filter. To compare the intensities, we scaled the 1D cross sections such that the $T_{1\rho}$-filtered spectrum does not exceed the intensity of the depectinated spectrum. For the 101-ppm cross section of Rha and GalA C1 (Fig. 8e), almost no intensity is retained in the $T_{1\rho}$-filtered spectrum, whereas strong intensity remains in the depectinated spectrum. Relative to the unfiltered spectrum of the intact CW, the $T_{1\rho}$-filtered spectrum was not scaled, whereas the depectinated spectrum was scaled down to 80%. For the 105-ppm cross section (Fig. 8d), the intensity of the 85-ppm peak relative to the 89-ppm peak is lower in the $T_{1\rho}$-filtered spectrum than in the unfiltered spectrum, confirming the preferential suppression of hemicellulose signals by the $T_{1\rho}$ filter. For both the 105-ppm and 62-ppm cross sections, the absolute intensities of the $T_{1\rho}$-filtered spectrum are about threefold lower than the unfiltered spectrum. Taken together, these results indicate that pectins represent only a subset of mobile components in the intact CW; hemicelluloses also possess substantial mobility, which makes them susceptible to suppression by the $T_{1\rho}$ filter so that the outcomes of the spectroscopic filter and chemical extraction of pectin are not identical.

### Implications of the SSNMR results on the structural role of pectins in primary CWs

The 2D and 3D SSNMR spectra and the relaxation times indicate that the central characteristic of pectin is its mobility. The partial removal of pectic polysaccharides is verified by monosaccharide analysis, quantitative $^{13}$C spectra, and INADEQUATE and spin diffusion spectra. The fact that the pectin signals are lower both in spectra that preferentially detect dynamic molecules and in spectra that preferentially detect rigid species indicates that the pectin intensity loss is a reflection of lower pectin amounts in the treated cell wall. The partial depectination caused an increase of cross peak intensities for the remaining polysaccharides in the

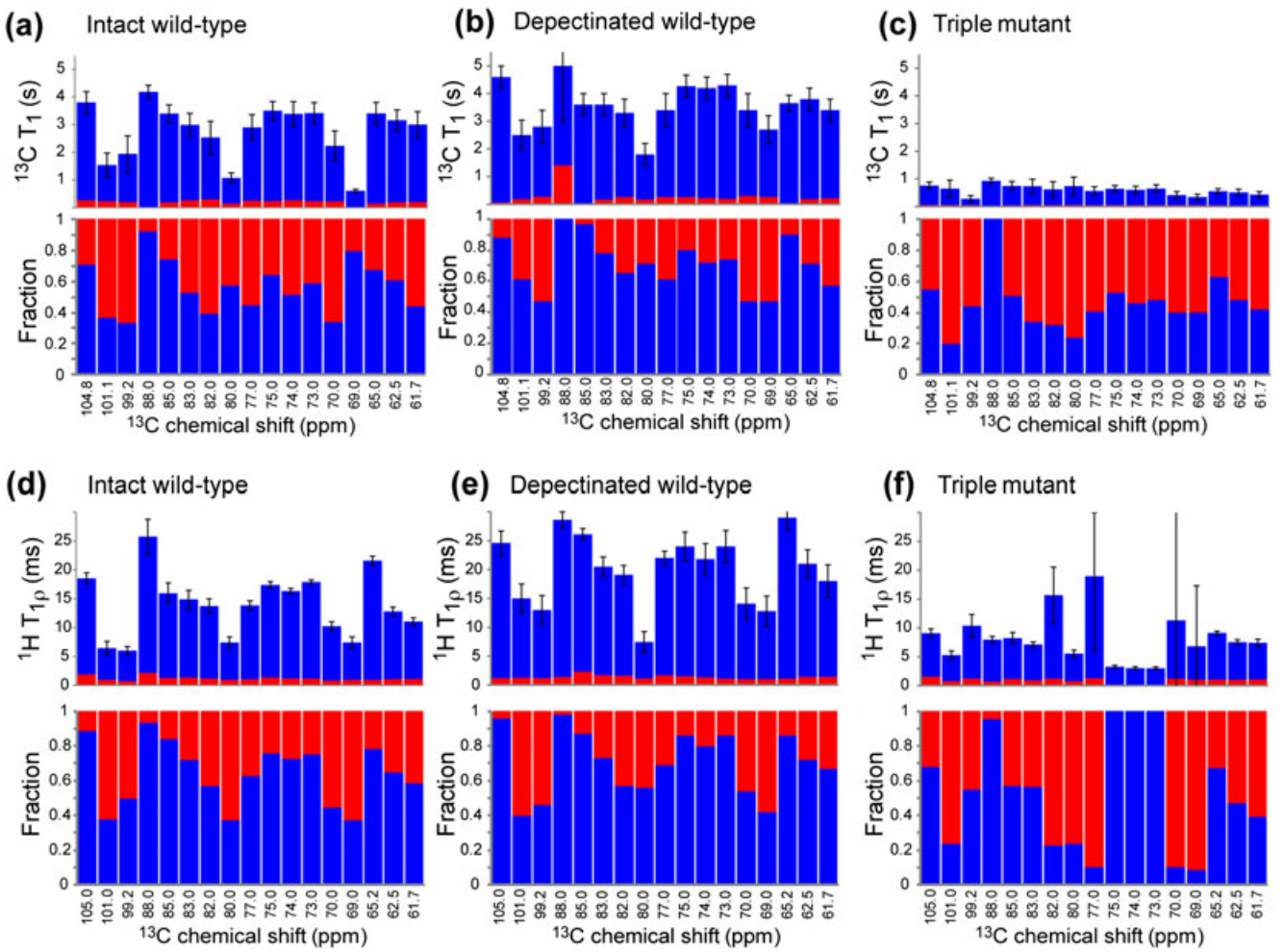


**Figure 6.** Complete $^{13}C$ $T_1$ (a-c) and $^{1}H$ $T_{1\rho}$ (d-f) relaxation times of (a, d) intact CW, (b, e) depectinated CW, and (c, f) XG-deficient triple mutant CW. Both the slow- (blue) and fast-relaxing (red) components are shown, and the corresponding fractions are plotted below the relaxation time diagrams. The depectinated CW has a lower fraction of the fast-relaxing components and much longer relaxation times than the intact CW, whereas the XG-deficient mutant has much shorter relaxation times than both wild-type cell walls.

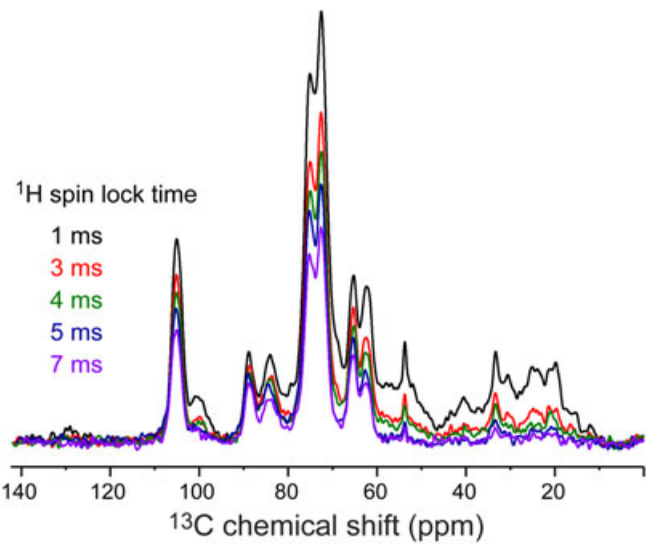


**Figure 7.** 1D $^{13}C$ CP-MAS spectra of the intact CW with varying $^{1}H$ spin-lock times. Spin lock preferentially suppresses the dynamic signals, which have short $T_{1\rho}$'s.

spin diffusion spectra, indicating increased rigidity of cellulose and hemicelluloses in the absence of a substantial portion of pectins. This qualitative interpretation is supported by the longer $^{13}C$ $T_1$ and $^{1}H$ $T_{1\rho}$ relaxation times for the depectinated CW (Figs 5, 6), showing that both nanosecond and microsecond timescale motions have slowed down for cellulose and XG in the depectinated CW compared with the intact CW. These relaxation times not only confirm the intensity changes in the 2D and 3D correlation spectra but also provide more quantitative and definitive evidence of the increased rigidity of the cell wall after partial pectin removal.

The conclusion of pectin dynamics in *Arabidopsis* are in excellent agreement with the findings about sugar beet CWs.[35] Based on $^{13}C$ NMR intensities as a function of the CP contact time, the previous study concluded that pectic galacturonans and arabinan chains were highly mobile. The contact time dependence of the $^{13}C$ intensities gave qualitative estimates of the $^{1}H$ $T_{1\rho}$ relaxation times, with the pectins having shorter $T_{1\rho}$s than cellulose and hemicelluloses, consistent with our quantitative $T_{1\rho}$ results.[12] Depectination also suppressed the signals of mobile residues in sugar beet CW. Because sugar beet CW has a much lower concentration of hemicelluloses than *Arabidopsis* CW, the similarity of

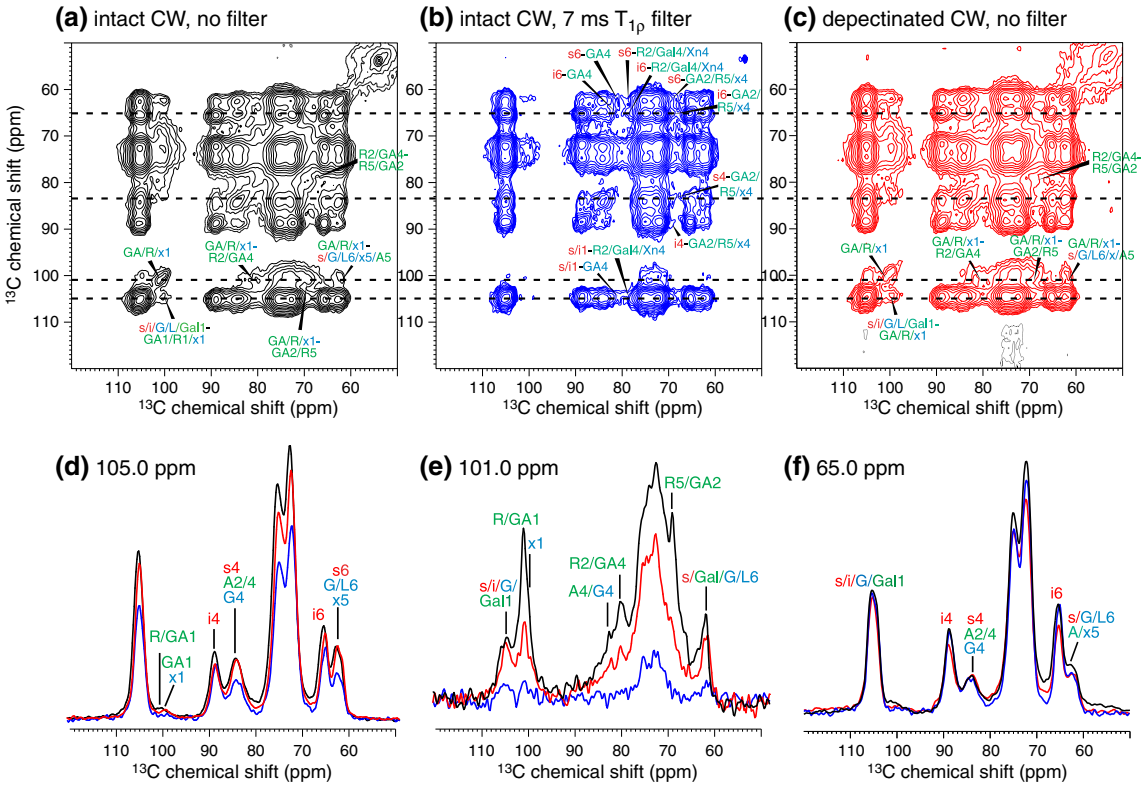


**Figure 8.** 2D $^{13}C$ PDSD spectra (300 ms) and 1D cross sections of CW samples with and without $^{1}H$ $T_{1\rho}$ filters. (a) Intact CW without any filter. (b) Intact CW with a 7 ms $T_{1\rho}$ filter. (c) Depectinated CW without any filter. (d) 105.0 ppm $\omega_1$ cross section. (e) 101.0 ppm $\omega_1$ cross section. (f) 65.0 ppm $\omega_1$ cross section.

these results indicates that the dynamic nature of pectins is general among many cell walls.

Based on the higher rigidity and cross peak intensities of the depectinated CW, we propose that pectin removal gives rise to more densely packed cellulose microfibrils by collapsing the space around them. Although it is difficult to separate the relative contributions of increased rigidity versus decreased intermolecular distances, we favor the model that higher rigidity results from more densely packed polysaccharide chains rather than a hollow network of rigid polymers. In this context, it is interesting to compare our results with an electron microscopy study of the primary CW of mature onion, a monocotyledon, before and after pectin extraction with a similar procedure.[36] The EM images of the intact CW showed a dense meshwork of long fibers of 5–12 nm diameter interspersed with ~10 nm diameter pores. After depectination, the pore sizes *increased* to 30–40 nm, whereas the fibers thickened and appeared to contain several microfibrils. We attribute this apparent discrepancy in the pore size change between our solid-state NMR results and the EM results to the different length scales probed by the two techniques. $^{13}C$ spin diffusion NMR probes intermolecular contacts on the sub-nanometer scale, which cannot be resolved using electron microscopy. Our model of denser packing of cellulose and hemicellulose reflects nanometer scale changes, which is in fact consistent with the thicker fibers observed in the depectinated onion CW.[36] In addition, the more mature CWs used in the EM study may have some structural differences from the 14-day old CWs used in the current study: the mature onion CW may contain more robust cellulose microfibrils that are less amenable to restructuring.

Various CW structural models proposed a pectin-hemicellulose network that was independent of a cellulose-hemicellulose network.[26] Although detailed features differ, these earlier models generally depicted pectins as spatially separate from cellulose by the intermediary XG chains. However, more recent evidence of pectin-cellulose,[37] pectin-XG,[38] pectin-phenolics,[39] and pectin-protein[40] interactions revises that notion. For example,

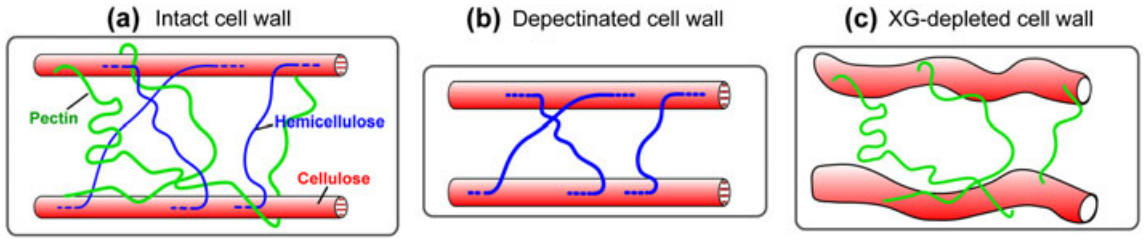


**Figure 9.** CW models derived from the solid-state NMR data. (a) Intact wild-type CW consists of rigid cellulose microfibrils separated from each other by dynamic pectin chains and semi-rigid hemicellulose that are partly embedded in the microfibril. (b) Partial depectination results in a more rigid and more densely packed CW with shorter distances between cellulose and hemicelluloses. (c) XG depletion by mutagenesis results in a CW with more dynamic cellulose and pectin chains.

pectins with neutral side chains, such as arabinans and galactans, bind to both commercial microcrystalline cellulose and native plant CW cellulose up to about 8-μg bound material per mg of cellulose.[37] Our recent solid-state NMR study suggest that the numbers of pectin-cellulose and XG-cellulose cross peaks in intact *Arabidopsis* CW are similar, indicating that on the molecular level, all three classes of polysaccharides exist in a single spatial network in the primary CW.[12] The observed denser packing of cellulose microfibrils after depectination also supports this single-network architecture.

The mobility of pectic polysaccharides is consistent with the highly branched structure of RG I and II.[41] It may be relevant for the well-known role of pectin in plant cell growth and elongation.[41,42] By keeping the rigid cellulose microfibrils apart, the mobile pectin chains may regulate wall porosity,[3,43] which would allow access of proteins and polysaccharides to different parts of the wall and to specialized regions such as intercellular junctions and air spaces.[5] The mobility of the pectins implies their existence in a less restrained and more solvent accessible environment, which may make them more prone to enzymatic digestion. This degradation may be prerequisite to cell wall restructuring and signaling.[41]

It is noteworthy that the effect of depectination on the CW structure is the opposite of the effect of XG depletion (Fig. 9). XG removal in the triple mutant CW drastically shortened $^{13}C$ $T_1$ and $^{1}H$ $T_{1\rho}$ relaxation times of both cellulose and pectins (Figs 5 and 6), indicating that the polysaccharides undergo faster motion in the absence of XG. Thus, although hemicellulose mobility is intermediate between that of cellulose and pectins,[12] its structural role in the CW is to enforce the rigidity of the wall, in contrast to pectins. Pectic polysaccharides are thought to form linkages to xyloglucans.[41] The necessary lack of such linkages in the hemicellulose-depleted mutant may also contribute to the increased flexibility of the CW.

This study demonstrates the ability of solid-state NMR in combination with isotopic labeling for investigating the molecular structures and dynamics of insoluble plant CWs in their native environment. The large number of cross peaks detected in 2D and 3D spectra confirms the ability of multidimensional MAS NMR to resolve intermolecular and intramolecular contacts in complex plant mixtures. Future application of this approach to plant CWs can be readily envisioned, such as investigating glycoprotein–polysaccharide interactions[44] and elucidating cellulose biosynthesis[45] for energy applications.

### Acknowledgement

This work was supported by the US Department of Energy, Office of Basic Energy Sciences, Division of Materials Sciences and Engineering under Award AL-90-360-001.

## References

[1] C. Somerville, S. Bauer, G. Brininstool, M. Facette, T. Hamann, J. Milne, E. Osborne, A. Paredez, S. Persson, T. Raab, S. Vorwerk, H. Youngs. Toward a systems approach to understanding plant cell walls. *Science* **2004**, *306*, 2206–2211.

[2] N. C. Carpita, M. McCann, The cell wall, in *Biochemistry and Molecular Biology of plants* (Eds: B. B. Buchanan, W. Gruissem, R. L. Jones), American Society of Plant Physiologists, Rockville, MD, **2000**.

[3] N. C. Carpita, D. M. Gibeaut. Structural models of primary cell walls in flowering plants: consistency of molecular structure with the physical properties of the walls during growth. *Plant J.* **1993**, *3*, 1–30.

[4] P. Sarkar, E. Bosneaga, M. Auer. Plant cell walls throughout evolution: towards a molecular understanding of their design principles. *J. Exp. Bot.* **2009**, *60*, 15–35.

[5] P. Albersheim, A. Darvill, K. Roberts, R. Sederoff, A. Staehelin, *Plant Cell Walls, Garland Science*, Taylor&Francis Group, LLC, New York, **2010**.

[6] E. Zablackis, J. Huang, B. Müller, A. G. Darvill, P. Albersheim. Characterization of the cell-wall polysaccharides of Arabidopsis thaliana leaves. *Plant Physiol.* **1995**, *107*, 1129–1138.

[7] C. J. Kennedy, G. J. Cameron, A. Sturcova, D. C. Apperley, C. Altaner, T. J. Wess, M. C. Jarvis. Microfibril diameter in celery collenchyma cellulose: X-ray scattering and NMR evidence. *Cellulose* **2007**, *14*, 235–246.

[8] M. Hedenström, S. Wiklund-Lindström, T. Oman, F. Lu, L. Gerber, P. Schatz, B. Sundberg, J. Ralph. Identification of lignin and polysaccharide modifications in Populus wood by chemometric analysis of 2D NMR spectra from dissolved cell walls. *Mol. Plant* **2009**, 933–942.

[9] F. Lu, J. Ralph. Non-degradative dissolution and acetylation of ball-milled plant cell walls: high-resolution solution-state NMR. *Plant J.* **2003**, *35*, 535–544.

[10] M. C. Jarvis. Self-assembly of plant cell walls. *Plant Cell Environ.* **1992**, *15*, 1–5.

[11] L. M. Davies, P. J. Harris, R. H. Newman. Molecular ordering of cellulose after extraction of polysaccharides from primary cell walls of Arabidopsis thaliana: a solid-state CP/MAS (13)C NMR study. *Carbohydrate Res.* **2002**, *337*, 587–593.

[12] M. Dick-Pérez, Y. Zhang, J. Hayes, A. Salazar, O. A. Zabotina, M. Hong. Structure and interactions of plant cell-wall polysaccharides by two- and three-dimensional magic-angle-spinning solid-state NMR. *Biochemistry* **2011**, *50*, 989–1000.

[13] M. Hong, Y. Su. Structure and dynamics of cationic membrane peptides and proteins: Insights from solid-state NMR. *Protein Sci.* **2011**, *20*, 641–655.

[14] A. E. McDermott. Structure and dynamics of membrane proteins by magic angle spinning solid-state NMR. *Annu. Rev. Biophys.* **2009**, *38*, 385–403.

[15] M. Renault, A. Cukkemane, M. Baldus. Solid-state NMR spectroscopy on complex biomolecules. *Angew. Chem. Int. Ed Engl.* **2010**, *49*, 8346–8357.

[16] R. Tycko. Molecular structure of amyloid fibrils: insights from solid-state NMR. *Q. Rev. Biophys.* **2006**, *39*, 1–55.

[17] A. G. Initiative. Analysis of the genome sequence of the flowering plant Arabidopsis thaliana. *Nature* **2000**, *408*, 796–815.

[18] S. C. Fry, Cell Wall Polysaccharide Composition and Covalent Crosslinking, in *Plant Polysaccharides: Biosynthesis and Bioengineering*. Annual Plant Reviews (Ed: P. Ulskov), **2011**, pp. 1–36.

[19] R. H. Atalla, D. L. VanderHart. Native Cellulose: A Composite of Two Distinct Crystalline Forms. *Science* **1984**, *223*, 283–285.

[20] T. J. Bootten, P. J. Harris, L. D. Melton, R. H. Newman. Solid-state (13)C NMR study of a composite of tobacco xyloglucan and Gluconacetobacter xylinus cellulose: molecular interactions between the component polysaccharides. *Biomacromolecules* **2009**, *10*, 2961–2967.

[21] K. M. Fenwick, D. C. Apperley, D. J. Cosgrove, M. C. Jarvis. Polymer mobility in cell walls of cucumber hypocotyls. *Phytochemistry* **1999**, *51*, 17–22.

[22] Y. Habibi, A. Heyraud, M. Mahrouz, M. R. Vignon. Structural features of pectic polysaccharides from the skin of *Opuntia ficus-indica* prickly pear fruits. *Carbohydrate Res.* **2004**, *339*, 1119–1127.

[23] T. J. Bootten, P. J. Harris, L. D. Melton, R. H. Newman. Solid-state 13C-NMR spectroscopy shows that the xyloglucans in the primary cell walls of mung bean (Vigna radiata L.) occur in different domains: a new model for xyloglucan-cellulose interactions in the cell wall. *J. Exp. Bot.* **2004**, *55*, 571–583.

[24] D. M. Cavalier, O. Lerouxel, L. Neumetzler, K. Yamauchi, A. Reinecke, G. Freshour, O. A. Zabotina, M. G. Hahn, I. Burgert, M. Pauly, N. V. Raikhel, K. Keegstra. Disrupting Two Arabidopsis thaliana Xylosyltransferase Genes Results in Plants Deficient in Xyloglucan, a Major Primary Cell Wall Component. *Plant Cell* **2008**, *20*, 1519–1537.

[25] O. A. Zabotina, W. T. van de Ven, G. Freshour, G. Drakakaki, D. Cavalier, G. Mouille, M. G. Hahn, K. Keegstra, N. V. Raikhel. Arabidopsis XXT5 gene encodes a putative alpha-1,6-xylosyltransferase that is involved in xyloglucan biosynthesis. *Plant J.* **2008**, *56*, 101–115.

[26] D. J. Cosgrove. Wall structure and wall loosening. A look backwards and forwards. *Plant Physiol.* **2001**, *125*, 131–134.

  

[27] D. Mohnen. Pectin structure and biosynthesis. *Curr. Opin. Plant Biol.* **2008**, *11*, 266–277.
[28] O. Zabotina, E. Malm, G. Drakakaki, V. Bulone, N. Raikhel. Identification and preliminary characterization of a new chemical affecting glucosyltransferase activities involved in plant cell wall biosynthesis. *Mol. Plant* **2008**, *1*, 977–989.
[29] M. Hohwy, H. J. Jakobsen, M. Eden, M. H. Levitt, N. C. Nielsen. Broadband dipolar recoupling in the nuclear magnetic resonance of rotating solids: a compensated C7 pulse sequence. *J. Chem. Phys.* **1998**, *108*, 2686–2694.
[30] A. Bax, R. Freeman, S. P. Kempsell. Natural-abundance 13C-13C coupling observed via double-quantum coherence. *J. Am. Chem. Soc.* **1980**, *102*, 4849–4851.
[31] S. Li, Y. Zhang, M. Hong. 3D 13C-13C-13C correlation NMR for de novo distance determination of solid proteins and application to a human alpha defensin. *J. Magn. Reson.* **2010**, *202*, 203–210.
[32] K. Takegoshi, S. Nakamura, T. Terao. C-13-H-1 dipolar-assisted rotational resonance in magic-angle spinning NMR. *Chem. Phys. Lett.* **2001**, *344*, 631–637.
[33] E. Gendreau, J. Traas, T. Desnos, O. Grandjean, M. Caboche, H. Hofte. Cellular basis of hypocotyl growth in Arabidopsis thaliana. *Plant Physiol.* **1997**, *114*, 295–305.
[34] D. Huster, L. S. Xiao, M. Hong. Solid-State NMR Investigation of the dynamics of colicin Ia channel-forming domain. *Biochemistry* **2001**, *40*, 7662–7674.
[35] C. M. G. C. Renard, M. C. Jarvis. A cross-polarization, magic-angle-spinning, $^{13}$C-nuclear-magnetic-resonance study of polysaccharides in sugar beet cell walls. *Plant Physiol.* **1999**, *119*, 1315–1322.
[36] M. C. McCann, B. Wells, R. K. . Direct visualization of cross-links in the primary plant cell wall. *J. Cell Science* **1990**, *96*, 323–334.
[37] A. W. Zykwinska, M. C. Ralet, C. D. Garnier, J. F. Thibault. Evidence for in vitro binding of pectin side chains to cellulose. *Plant Physiol.* **2005**, *139*, 397–407.
[38] J. E. Thompson, S. C. Fry. Evidence for covalent linkage between xyloglucan and acidic pectins in suspension-cultured rose cells. *Planta* **2000**, *211*, 275–286.
[39] T. Ishii, T. Tobita. Structural characterization of feruloyl oligosaccharides from spinach-leaf cell walls. *Carbohydr. Res.* **1993**, *248*, 179–190.
[40] M. J. Kieliszewski, D. T. A. Lamport, L. Tan, M. C. Cannon, Hydroxyproline-rich Glycoproteins: Form and Function, in *Plant Polysaccharides* (Ed: P. Ulvskov), Biosynthesis and Bioengineering, Annaul plant reviews, **2011**, pp. 321–336.
[41] K. H. Caffall, D. Mohnen. The structure, function, and biosynthesis of plant cell wall pectic polysaccharides. *Carbohydr. Res.* **2009**, *344*, 1879–1900.
[42] S. Bouton, E. Leboeuf, G. Mouille, M. T. Leydecker, J. Talbotec, F. Granier, M. Lahaye, H. Höfte, H. N. Truong. QUASIMODO1 encodes a putative membrane-bound glycosyltransferase required for normal pectin synthesis and cell adhesion in Arabidopsis. *Plant Cell* **2002**, *14*, 2577–2590.
[43] M. C. Jarvis, S. P. H. Briggs, J. P. Knox. Intercellular adhesion and cell separation in plants. *Plant Cell Environ.* **2003**, *26*, 977–989.
[44] D. J. Cosgrove. Growth of the plant cell wall. *Nat. Rev. Mol. Cell Biol.* **2005**, *6*, 850–861.
[45] T. J. Bootten, P. J. Harris, L. D. Melton, R. H. Newman, Using Solid-State 13C NMR Spectroscopy to Study the Molecular Organisation of Primary Plant Cell Walls, in *The Plant Cell Wall: Methods and Protocols* (Ed: Z. A. Popper), Methods in Molecular Biology, Springer Science, **2011**, pp. 179–196.

# Supporting Information

## Multidimensional Solid-State NMR Studies of the Structure and Dynamics of Pectic Polysaccharides in Uniformly $^{13}$C-Labeled *Arabidopsis* Primary Cell Walls

Marilu Dick-Perez[1], Tuo Wang[1], Andre Salazar[2], Olga A. Zabotina[2], and Mei Hong[1]*

[1]Department of Chemistry and the Ames Laboratory, [2]Department of Biochemistry, Biophysics & Molecular Biology, Iowa State University, Ames, IA 50011

**Table S1**. Conditions of the SSNMR experiments for characterizing *Arabidopsis* CWs.

| Experiment | Sample | Mixing time (ms) | Polariza-tion | Temp (K) | MAS rate (kHz) | Recycle delay (s) |
|---|---|---|---|---|---|---|
| 1D $^{13}$C DP | Intact & treated | - | DP | 294 | 7 | 25 |
| 2D J-INADEQUATE | Intact | 6 | DP | 295 | 12 | 2 |
| 2D J-INADEQUATE | Treated | 6 | DP | 295 | 11.8 | 1.8 |
| 2D DQ filtered CC | Intact | 1.14 | CP | 296 | 7.0 | 1.7 |
| 2D DQ filtered CC | Treated | 1.33 | CP | 296 | 7.5 | 1.8 |
| 3D CCC | Intact | 8, 300 | CP | 273 | 12.0 | 1.8 |
| 3D CCC | Treated | 8, 300 | CP | 296 | 9.3 | 1.85 |
| 2D DARR | Intact | 8 | CP | 293 | 7.5 | 1.8 |
| 2D DARR | Treated | 8 | CP | 293 | 7.5 | 1.8 |
| 2D PDSD | Intact | 300 | CP | 293 | 7.5 | 1.8 |
| 2D PDSD, 7 ms $T_{1\rho}$ filter | Intact | 300 | CP | 293 | 7.5 | 2.0 |
| 2D PDSD | Treated | 300 | CP | 293 | 7.5 | 2.1 |
| 2D PDSD | Intact | 300 | CP | 298 | 9.3 | 1.9 |
| 2D PDSD | Treated | 300 | CP | 298 | 9.3 | 1.9 |

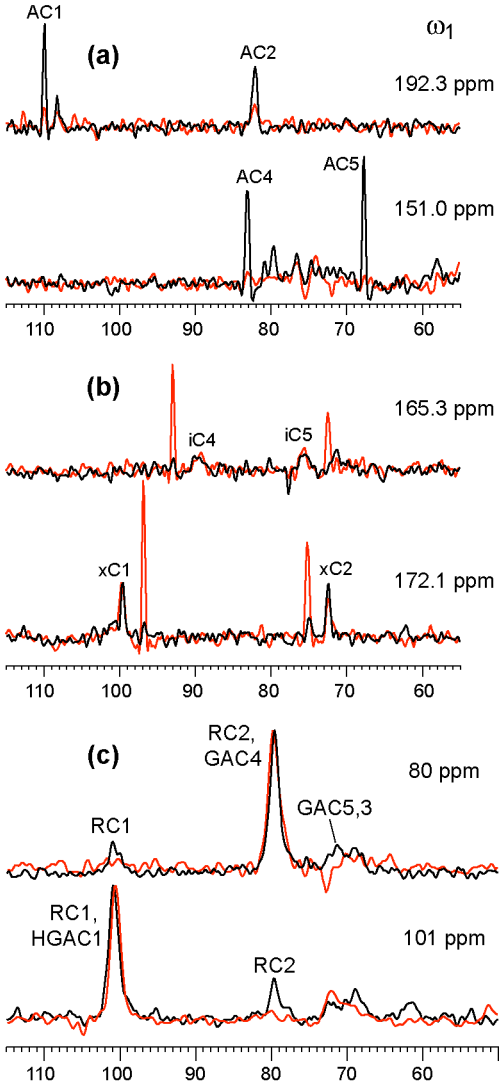


**Figure S1**. Representative 1D cross sections of 2D $^{13}C$-$^{13}C$ correlation spectra of intact (black) and depectinated (red) primary CWs to compare cross peak intensities. (a, b) 1D cross sections from DP J-INADEQUATE spectra of Figure 2(a, b). The $\omega_1$ double-quantum chemical shifts of the cross sections are indicated. The 192 ppm and 151 ppm cross sections in (a) show the removal of pectin peaks in the depectinated CW. The 165 and 172 ppm cross sections in (b) show additional cross peaks in the depectinated CW that are absent in the WT cell wall. (c) 1D cross sections from the 2D DQ filtered spectra of Figure 2(c, d). The depectinated CW shows weaker intensities for pectin cross peaks.

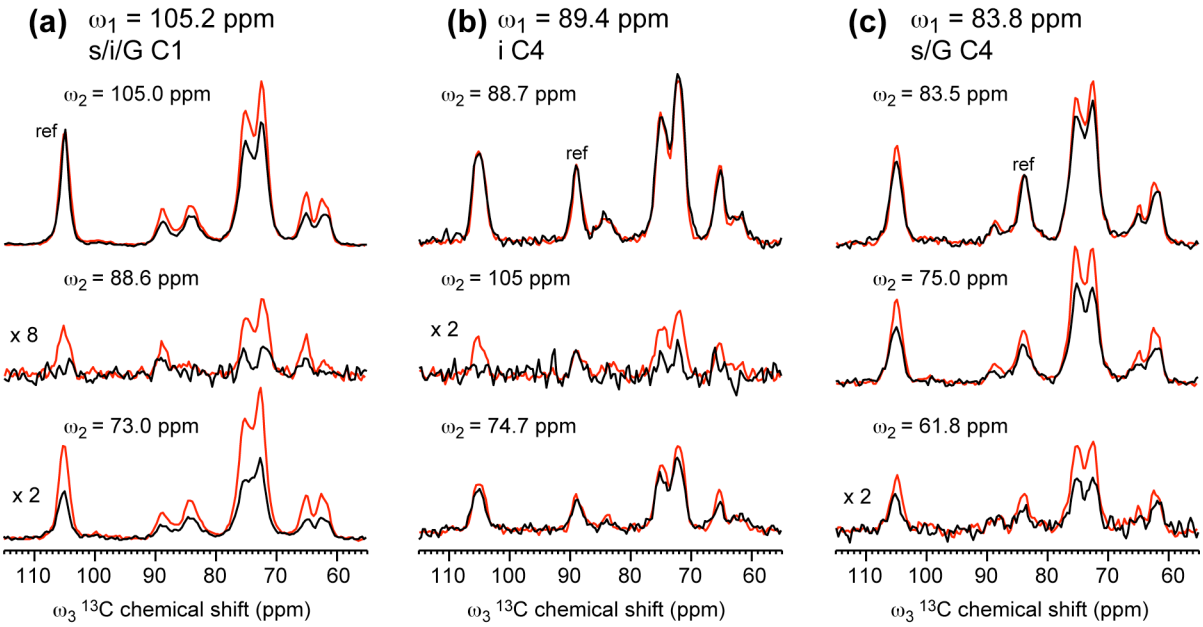


**Figure S2.** Selected 1D cross sections from the 3D CCC spectra shown in Figure 4 for the intact (black) and depectinated (red) CW. (a) $\omega_1$=105 ppm 2D plane (Figure 4a). The 105 ppm cross section serves as the reference while the 89 ppm and 73 ppm $\omega_2$ cross sections show the increased cross peak intensity of the depectinated CW. The cross sections of the two samples are scaled such that the intensity of the triple diagonal peak at (105, 105, 105) ppm (labeled as ref) is the same. (b) $\omega_1$ = 89 ppm 2D plane (Figure 4b). The depectinated CW has higher iC4 to iC1 and iC3/C5 cross peaks. The cross sections of the two samples are scaled such that the triple diagonal peak at (89, 89, 89) ppm (labeled as ref) has the same intensity. (c) $\omega_1$=83.8 ppm 2D plane (Figure 4a). The cross sections of the two samples are scaled such that the triple diagonal peak at (84, 84, 84) ppm (labeled as ref) has the same intensity. The depectinated sample shows higher cross peak from s/G C4 to s/G C1 and C3/5.

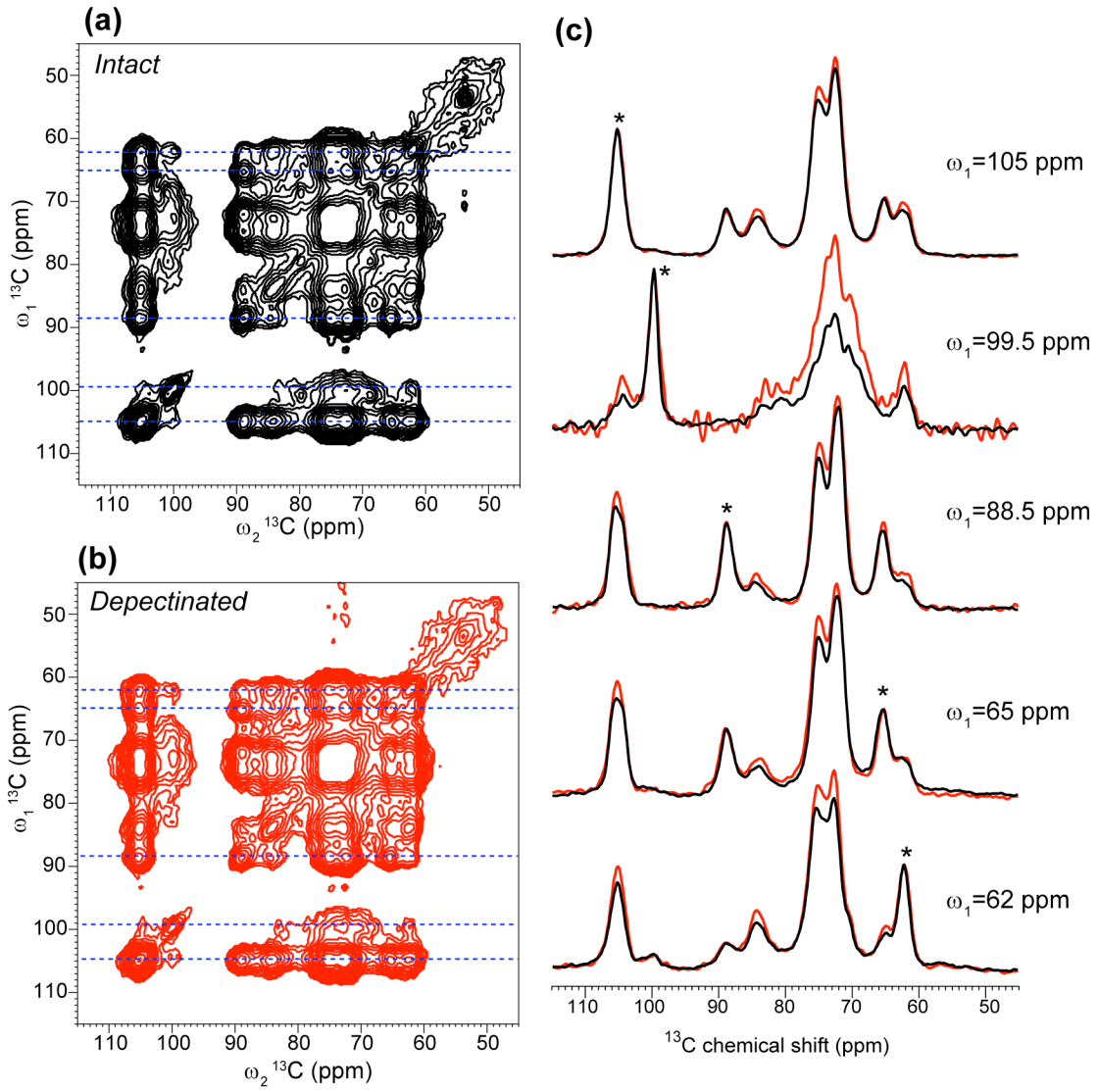


**Figure S3**. 2D $^{13}C$-$^{13}C$ PDSD spectra with 300 ms mixing measured at 298 K under 9.3 kHz MAS. (a) 2D spectrum of the intact CW. (b) 2D spectrum of the depectinated CW. (c) 1D cross sections from the 2D spectra at the indicated $\omega_1$ chemical shifts, illustrating the higher cross peak intensities of the depectinated CW. Cross sections are scaled such that the diagonal peak (indicated by *) has equal intensity between the two spectra. The depectinated CW sample shows stronger cross peaks for most cross sections as a result of more efficient spin diffusion for the more rigid polysaccharides that remain in the cell wall.

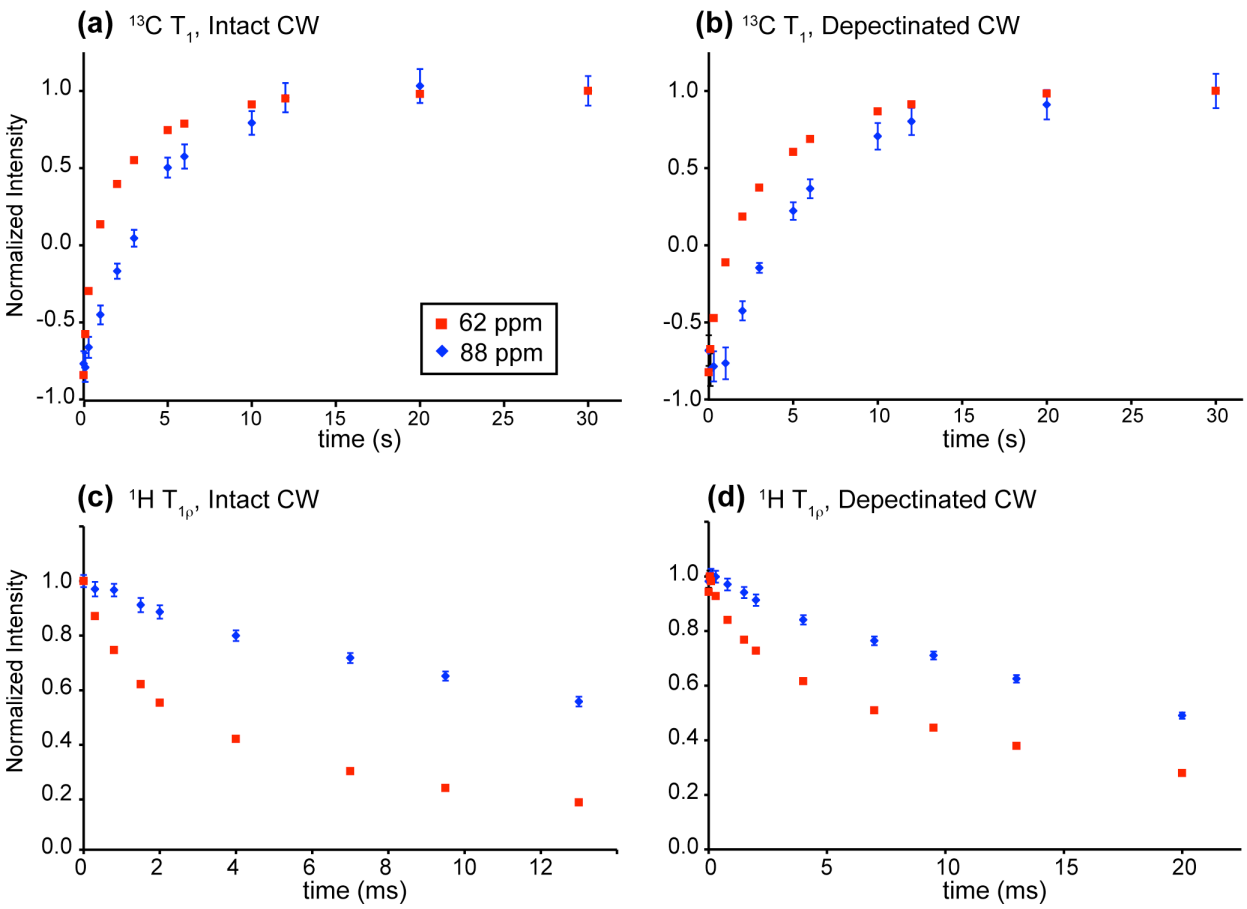


**Figure S4.** Representative relaxation data used to obtain the $^{13}$C T$_1$ (a, b) and $^{1}$H $T_{1\rho}$ values (c, d) of the intact (a, c) and depectinated (b, d) CW samples. The 88 ppm and 62 ppm peaks of interior cellulose C4 and surface cellulose and XG backbone C6 are shown. Note the different time axis for the $^{1}$H $T_{1\rho}$ data between (c) and (d).